Elsevier Editorial System(tm) for Tribology International

Manuscript Draft

Manuscript Number:

Title: Effects of surface texture deterioration and wet surface conditions on asphalt runway skid resistance

Article Type: Full Length Article

Keywords: Finite element analysis; hydroplaning; friction deterioration; pavement surface texture.

Corresponding Author: Dr. Xingyi Zhu,

Corresponding Author's Institution: Key Laboratory of Road and Traffic Engineering of Ministry of Education

First Author: Xingyi Zhu

Order of Authors: Xingyi Zhu; Yang Yang; Hongduo Zhao; Denis Jelagin; Feng Chen; Francisco A. Gilabert; Alvaro Guarin

Abstract: The friction force for aircraft landing is mainly provided by the texture of runway surfaces. Worn-out surfaces along with wet conditions increase the risk of poor control during aircraft landing. Accordingly, this study investigated three types of asphalt runways. Surface texture deterioration was simulated using a surface texture wear algorithm. Kinematic friction models were established based on the viscoelastic property of rubber materials, power spectrum density, and statistics of surface textures. A finite element model was developed by considering a real rough runway surface and different water film depths. The effects of different factors, such as velocity, wear ratio, runway type, water film depth, and slip ratio, on the skid resistance of the runway were analyzed.

Suggested Reviewers: Baoshan Huang
The University of Tennessee
bhuang@utk.edu

Qingli Dai
Michigan Technological University
qingdai@mtu.edu

Yuhong Wang
The Hong Kong Polytechnic University
yuhong.wang@polyu.edu.hk

Cover Letter

Dr. Xingyi Zhu
Key Laboratory of Road and Traffic Engineering of Ministry of Education, Tongji University
Tel: 86-18817459401
Email:zhuxigyi66@aliyun.com

Re: Manuscript submitted to ***Tribology International***
Title: **Effects of surface texture deterioration and wet surface conditions on asphalt runway skid resistance**

Authors: Xingyi Zhu, Yang Yang, Hongduo Zhao*, Denis Jelagin, Feng Chen, Francisco A. Gilabert, Alvaro Guarin

May 8, 2020

Dear Editor-in-Chief,

We are submitting our manuscript titled, "**Effects of surface texture deterioration and wet surface conditions on asphalt runway skid resistance**" for your kind consideration of its suitability for publication in ***Tribology International*** as a full length article. We affirm here that the results presented in the paper are original and have not been published or submitted elsewhere.

I look forward to hearing from you soon. With best regards,

Sincerely yours,

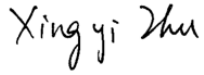

Zhu Xingyi

* Corresponding author. E-mail: hdzhao@tongji.edu.cn

Statement of Originality

The work contained in this manuscript has not been previously submitted for a degree or diploma at any other higher education institution. To the best of my knowledge and belief, the manuscript contains no material previously published or written by another person except where due references are made.

Highlights

- Runway surface texture deterioration was considered in FEM simulation based on a surface texture wear algorithm.
- The kinematic friction coefficient between tire rubber and runway was calculated based on real 3D microstructure of surface texture and power spectral density.
- The effect of surface texture deterioration and water-covered conditions were considered simultaneously in finite element model.

Effects of surface texture deterioration and wet surface conditions on asphalt runway skid resistance

Xingyi Zhu[1], Yang Yang[1], Hongduo Zhao[1*], Denis Jelagin[2], Feng Chen[2], Francisco A. Gilabert[3], Alvaro Guarin[2]

[1]Key Laboratory of Road and Traffic Engineering of Ministry of Education, Tongji University, Shanghai 200092, P. R. China

[2] Department of Civil and Architectural Engineering, KTH Royal Institute of Technology, Brinellvägen 23, 10044 Stockholm, Sweden

[3] Ghent University, Mechanics of Materials and Structures, Tech Lane Ghent Science Park – Campus A, Technologiepark-Zwijnaarde 46, Zwijnaarde, 9052 Ghent, Belgium

Abstract

The friction force for aircraft landing is mainly provided by the texture of runway surfaces. The mechanism underlying friction force generation is the energy dissipation of tire rubber materials during random excitation induced by asperities. However, the runway surface texture is deteriorated by cyclic loading and environmental effects during the service life of a runway, leading to loss of braking force and extension of landing distance. Additionally, when an aircraft lands on a wet runway at a high velocity, the hydrodynamic force causes the tires to detach from the runway surface, which is risky and may lead to the loss of aircraft control and runway excursion. Worn-out surfaces along with wet conditions increase the risk of poor control during aircraft landing. Accordingly, this study investigated three types of asphalt runways (SMA-13, AC-13, and OGFC-13). Surface texture deterioration was simulated using a surface texture wear algorithm. Kinematic friction models were established based on the viscoelastic property of rubber materials, power spectrum density, and statistics of surface textures. A finite element model was developed by considering a real rough runway surface and different water film depths. The effects of different factors, such as velocity, wear ratio, runway type, water film depth, and slip ratio, on the skid resistance of the runway were analyzed.

* Corresponding author. E-mail: hdzhao@tongji.edu.cn

Key words:

Finite element analysis; hydroplaning; friction deterioration; pavement surface texture; pavement reconstruction.

1 Introduction

During recent years, dozens of runway excursion accidents occur each year on average, causing considerable damage to the aircraft fuselage. Ensuring aircraft landing safety is crucial, particularly on wet or worn-out runways. Studies have demonstrated that friction force is considerably reduced on worn-out runways [1-3]. Moreover, numerous studies have reported that landing at high speed under wet weather conditions could cause traction failure [4-6]. However, current approaches for evaluating runway skid resistance are based on periodic friction measurement. In such approaches, the wet condition of runway surfaces and the deterioration of surface textures cannot be considered.

Numerous factors influence skid resistance performance, such as runway surface conditions (surface texture, runway surface material properties, and water films), tire conditions (tire rubber, tread pattern, attrition rate, tire pressure, and load), landing speed, and ambient temperature. Surface texture is a major factor influencing runway skid resistance. Kanafi investigated the relationship among the friction, macrotexture, and microtexture of asphalt pavements by conducting a 9-month observation; some statistical indicators and fractal parameters were used to associate surface texture with friction values [3]. Zelelew used wavelet tools to analyze the influence of macro-texture properties on the skid resistance of asphalt roads [7]. Bitelli obtained road surface texture morphology by using a laser scanner and then compared both two-dimensional and three-dimensional (3D) indicators by evaluating surface roughness; the results revealed that the surface texture of roads deteriorated considerably with an increase service life and engendered a 10%–15% skid resistance loss after only 5 months of use [8]. Moreover, several studies have demonstrated that the skid resistance of runways decreases considerably under wet weather conditions [3, 9-14]. According to statistical analysis results in a previous study, wet-pavement friction is highly relevant to traffic crashes on highways [15]. However, Kumar reported that satisfactory macrotexture can enhance driving safety in wet weather by improving the skid resistance of roads [16]. Fwa proved that trapezoidal-grooved runways could substantially

improve aircraft safety in wet weather [6].

The National Aeronautics and Space Administration (NASA) was the first to conduct on-site hydroplaning experiments. On the basis of these experiments, Dreher proposed a formula for estimating hydroplaning speed [17]. Harwood reported that slightly wet pavements can engender 75% tire-pavement friction loss compared with dry roads and roads with a clean surface [18]. For high-speed vehicles, even a thin water film on the road is sufficient to produce hydroplaning. Moreover, other factors, such as tread wear, tire groove depth, and surface texture, have been considered in skid resistance formulas developed through experimental approaches [19, 20]. However, such experimental approaches are highly expensive and time consuming. Furthermore, field tests can seldom reveal complex interactions between multiple influence factors. With advancements in numerical simulations, finite element (FE) methods have become a complementary approach for clarifying influencing parameters.

With actively use of FE methods, effects of multiple influence factors have been studied by researchers. Zmindak introduced an FE approach for analyzing braking capability and hydroplaning probability during airplane landing [21]. Fwa and Ong developed a hydroplaning FE model based on solid mechanics and fluid dynamics. They investigated the phenomenon of hydroplaning by considering multiple influencing factors, including tire tread pattern, vehicle velocity, and water depth [22-25]. Additionally, the hydroplaning speed obtained from their model was verified using empirical formulations established by NASA [22, 23]. Anupam and Srirangam improved the aforementioned FE model in two aspects. The improved model can simulate water splashing through a coupled Eulerian–Lagrangian (CEL) algorithm [26]. They also developed a pavement texture model through computed tomography scanning and 3D reconstruction processes of asphalt mixtures [27, 28]. Huang has presented a framework for computing braking distance based on a whole-car simulation model and tire FE analysis [29, 30]. Studies on FE methods have revealed the hydroplaning process and interactions of many factors; however, few studies have investigated the influence of pavement texture deterioration in their numerical models.

Current FE studies on the hydroplaning phenomenon have two limitations. First, the empirical friction models used in FE studies oversimplify the interaction between tread rubber and pavement, causing difficulties in quantifying the skid resistance properties of pavements with different textures. Second, FE studies have applied fixed friction models without considering that

friction coefficients would decay with runway use. To address these limitations, the present study developed an algorithm for simulating the wearing deterioration of runway textures. The study established a friction model by considering adhesion and hysteresis friction forces between tread rubber and runways. Subsequently, an FE framework was proposed to investigate tire landing on worn-out and water-covered runways in order to determine runway skid resistance performance. Moreover, the influence of various factors on skid resistance was investigated using the FE framework.

2 FE model

Fig. 1 illustrates the framework of the aircraft hydroplaning model developed int his study. The hydroplaning model comprises four submodels: tire, runway, interaction, and water film models. The tire model is based on aircraft tire geometry data and material properties. A runway surface profile was obtained to develop a rough runway model. The surface profile was further deteriorated programmatically to simulate surface texture evolution with time period of use. Subsequently, the power spectral density (PSD) of the runway surface and complex modulus of rubber were obtained to evaluate the friction between the tire and runway. Finally, the water film model was developed according to an Eulerian algorithm. The hydrodynamic force could be obtained through the tire-water film-runway surface model. The friction loss caused by the hydrodynamic force was then analyzed.

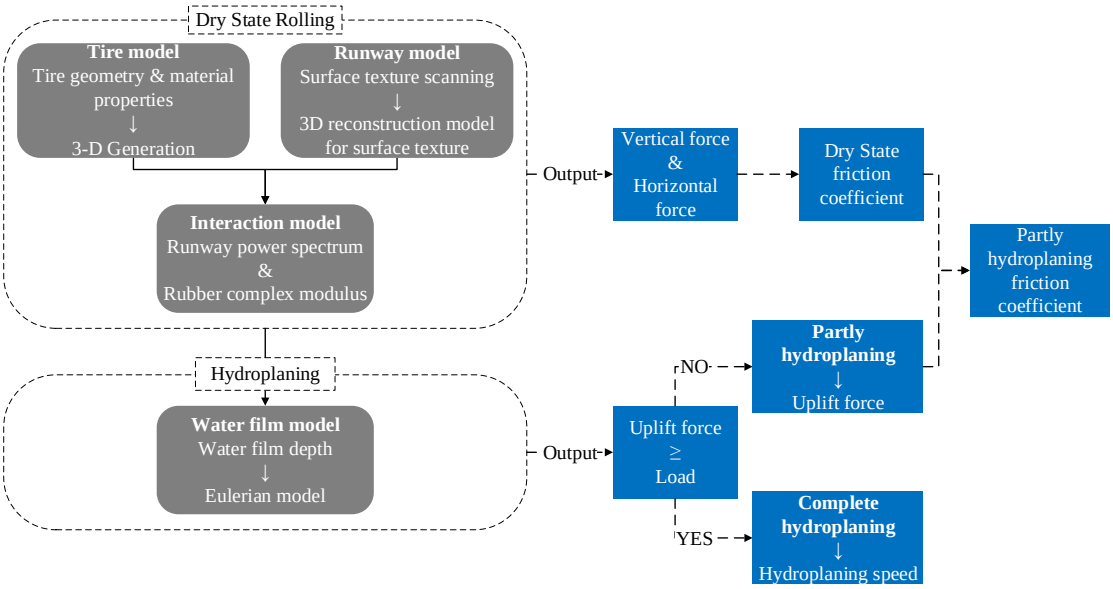

Fig. 1. Framework of hydroplaning model for wet runway.

2.1 Modeling of tire and water film

Tire modeling is a key component of skid resistance and hydroplaning simulations. In this study, a tire on the main wheel of an Airbus A320 aircraft, a mainstream aircraft, was used for tire modeling in the FE simulation. Such a tire, namely a 46 × 17.0 R20 type tire, exhibits a tread width and diameter of 43.24 and 116.84 cm, respectively. The tread has four grooves with a width and depth of 9 and 10 mm, respectively, for water drainage. In the tire model in this study, a landing load and maximum landing speed of 6600 kg and 205 km/h, respectively, were set. Table 1 presents the structural parameters of a typical 46 × 17.0 R20 tire on the main wheel of an A320 aircraft.

Table 1. Parameters of tire on the main wheel of A320 craft.

Parameter	Values	Parameter	Values
Tire type	46×17.0R20	Landing load (kg)	6600
Tire Pressure (kPa)	1147	Number of grooves	4
Diameter (mm)	1168	Tread pattern	Circumferential grooves
Width of tire (mm)	432	Width of grooves (mm)	9
Maximum speed (km/h)	205	Depth of grooves(mm)	10

Fig. 2 illustrates the FE model of tire hydroplaning. A tire is primarily composed of a rubber and a cord layer. The rubber provides deformation and abrasion resistance, and the cord layer is

the skeleton of the tire that sustains load and absorbs shocks. The tire rubber comprises sidewall rubber, shoulder rubber, tread rubber, under tread rubber, and inner liner rubber, all of which differ slightly in mechanical properties. The cord layer material mainly comprises steel and polyester cords and includes a belt layer, cap layer, carcass layer, bead, and submouth cloth. Some materials with similar properties were combined in this study to simplify the FE model. Therefore, the materials used in this model were the tread rubber, sidewall rubber, under tread rubber, inner liner rubber, shoulder rubber, belt layer, crown layer, body ply layer, and bead layer. Table 2 presents the hyperelastic material properties of the tire rubber and elastic material properties of the cord layer. To obtain precise results, the tire tread was fine meshed to match a runway mesh.

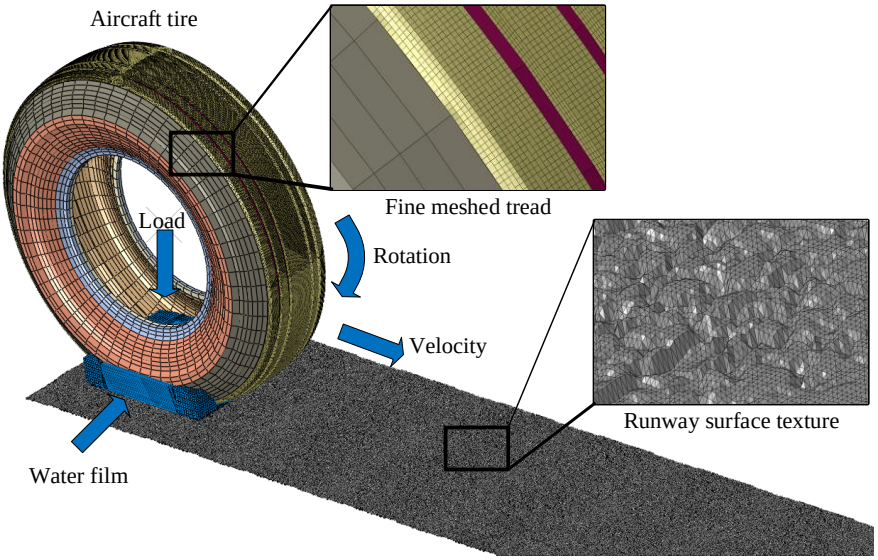

Fig. 2. Hydroplaning model of aircraft tire.

Table 2. Properties of tire materials.

Rubber materials	Yeoh model[30]			
	C_{10}	C_{20}	C_{30}	D_i (i=1, 2, 3)
Tread	1.200201	-1.20439	0.945575	0
Under Tread	0.451268	-0.15744	0.080273	0
Sidewall	0.470942	-0.16431	0.083773	0
Shoulder	0.445972	-0.1556	0.079331	0
Inner liner	0.486342	-0.16968	0.086513	0
Cord layer materials	Young's modulus (MPa)		Poisson's ratio	
Belt layer	20000		0.33	
Crown layer	2000		0.45	
Body ply layer	5000		0.45	

Bead layer	80000	0.33

The CEL algorithm was employed for fluid–solid coupling analysis, with the solid tire and water film being investigated using the Lagrangian and Eulerian elements, respectively. The CEL algorithm prevents excessive element distortion caused by the Lagrangian elements. It can determine the motion interface of water by using the Eulerian elements. The Eulerian model requires both the water film and air layers to capture the water motion in hydroplaning. In this study, an Eulerian model measuring 1000 × 600 × 50 mm^3 was developed. The size of the Eulerian model should sufficiently cover the tire footprints and leave adequate room for water splashing during landing. The water layer under the tire footprints was meshed with a size of 1 mm to obtain accurate hydrodynamic results. A pump area and an outlet were set in the front and back of the water film model, respectively, to provide constant fluids at a certain speed.

2.2 Runway surface model

Stone mastic asphalt (SMA-13) is commonly used as an surfacing material for ungrooved runways at airports. To consider the effect of surface texture variations on skid resistance, two other different asphalt mixture types, namely asphalt concrete (AC-13) and open-graded friction course (OGFC-13), were prepared in this study. Table 3 presents the gradation and basic properties of the three types of asphalt mixtures. The specimens, measuring 300 × 300 × 50 mm^3, were prepared using the wheel grinding method. Subsequently, the prepared specimens were cut into a size of 200 × 100 × 50 mm^3 according to the requirements of scanning equipment. The surface textures of the mixtures were determined using a KEYENCE VR-5000 optical scanning instrument (Japan) with a 0.1-mm resolution (Fig. 3). The mean profile depth (MPD) is a commonly used indicator in the analysis of surface roughness. Root mean square (RMS) is also an indicator for assessing the deviation of asperities from the central line of the surface texture. Both indicators are highly correlated with runway skid resistance. In this study, the OGFC-13 and AC-13 specimens exhibited the highest and lowest MPD and RMS, respectively (Table 3), which was mainly caused by aggregate gradation. OGFC was designed to be water permeable; it exhibited the largest coarse aggregate proportion and thus the highest RMS and MPD. SMA was designed for stone–stone contact within the mixture to improve tire grip. Compared with AC, SMA comprised a higher content of coarse aggregates; thus, the RMS and MPD of SMA values

were higher than those of AC.

Table 3. Gradation and basic properties of asphalt mixture specimens.

Mixture Type	Sieving Size (mm)									
	16	13.2	9.5	4.75	2.36	1.18	0.6	0.3	0.15	0.075
	Passing Ratio (%)									
AC-13	100	98.9	83.8	43.4	29.8	22.8	17.6	10.1	8.1	5.9
SMA-13	100	96.4	63.6	24.6	21.6	18.5	15.9	12.2	11.3	10.3
OGFC-13	100	98.6	78.6	25.4	11.5	9.5	8.5	7.1	6.5	5.5

Mixture Type	Asphalt Aggregate Ratio (%)	Air Void (%)	RMS (mm)	MPD (mm)	Asphalt Binder
AC-13	4.6	4.9	1.94	0.65	AH-70
SMA-13	5.25	3.7	2.11	0.80	SBS modified asphalt
OGFC-13	4.7	20.5	3.21	1.08	High-Viscosity asphalt

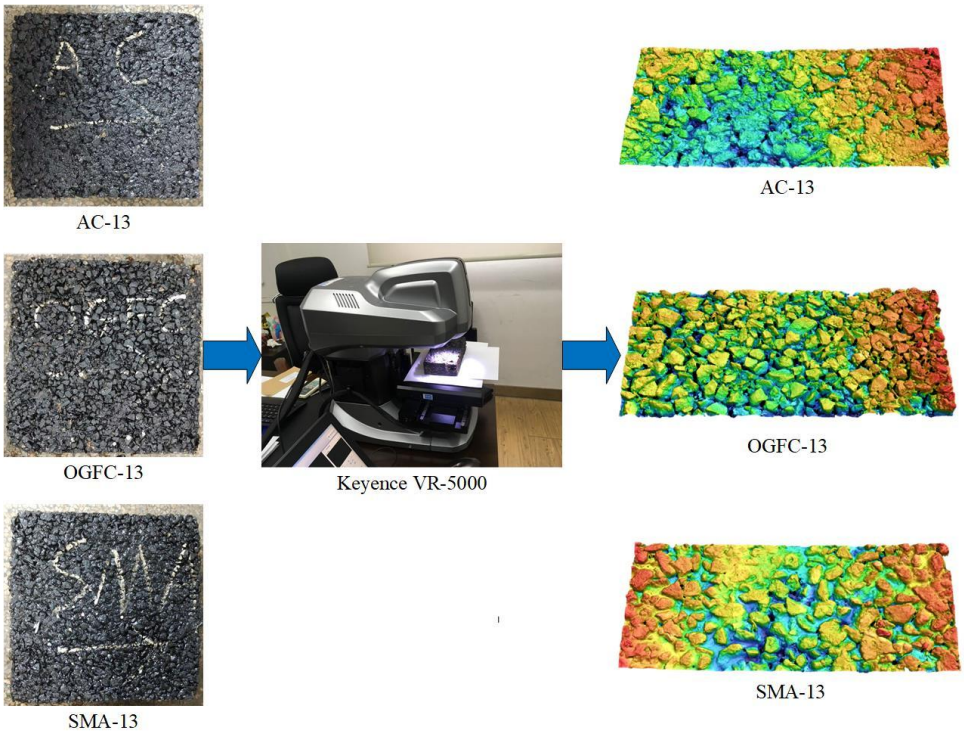

Fig. 3. Optical scanning of asphalt mixture.

After a runway is used for a certain period, the surface texture would deteriorate because of constant landing loads. In this study, the asperity height decreased globally after a certain period of use, as presented in Fig. 4. Nevertheless, high asperities exhibited greater height loss than did low asperities. After a certain number of passes, the observed surface texture became relatively smooth. However, obtaining the evolution of surface texture at the same runway site is typically

difficult. Therefore, this study developed an algorithm to simulate the wear of airport pavements after long-term use. To quantify the texture of runway surfaces, the height amplitude can be measured within a sample. Consider, for example, a line-scanning height (Fig. 5); the pavement texture comprises asperities of varying size. The highest asperities are subjected to substantially larger stress than lower asperities when an aircraft lands and brakes. Therefore, the highest asperities would be worn out faster than would lower asperities. Moreover, asperities whose height is below a certain threshold would not be subject to wear because they cannot establish contact with the tire. On the basis of the aforementioned description, the surface texture can be deteriorated programmatically using the following algorithm:

$$T = (Z_{max} - Z_{min}) \times \frac{w_r}{100} \tag{1}$$

$$Z = (Z - T) \times \frac{w_r}{100} + T \; if \; Z > T \tag{2}$$

where w_r represents the wear ratio (i.e., the wear degree). For example, a w_r value of 10 indicates that 10% of the highest asperities are polished. T is the threshold, and asperities below a set threshold would not be deteriorated. Z is the asperity height. Z_{max} and Z_{min} represent the highest and lowest asperities, respectively. Fig. 6 presents the profiles of worn-out runways with different wear ratios, indicating RMS values obtained for six surface profiles to be 2.11, 2.10, 2.09, 2.05, 1.79, and 1.25.

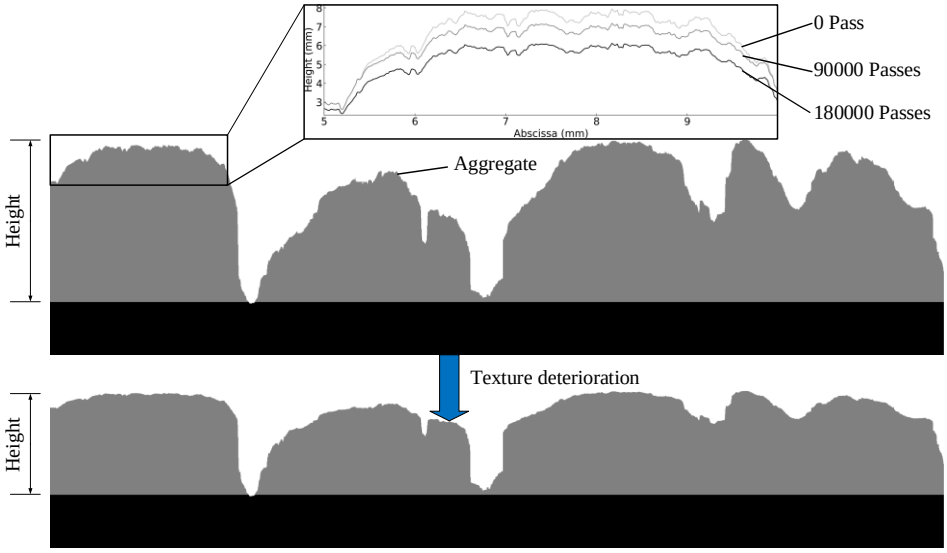

Fig. 4. Evolution of surface texture.

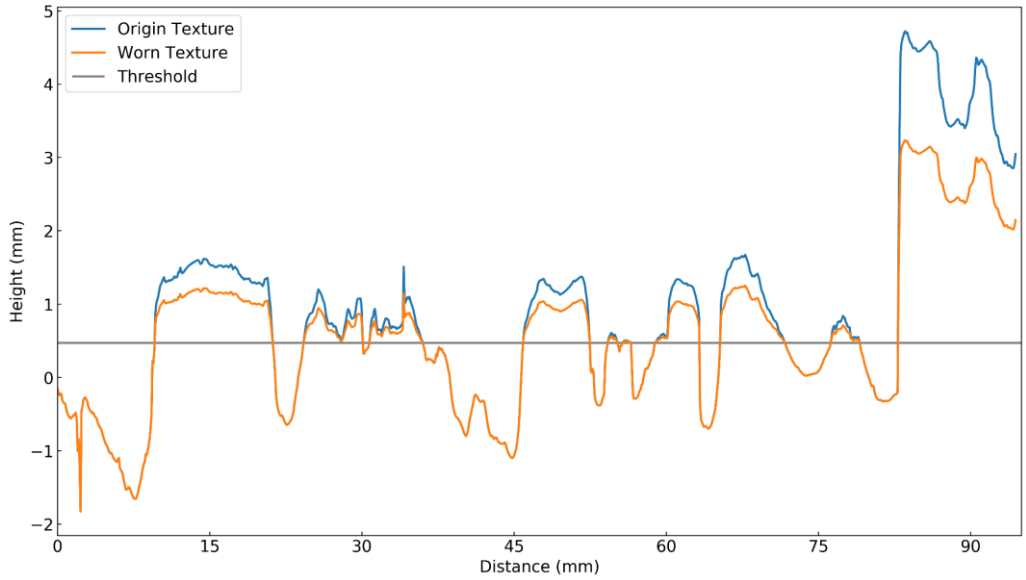

Fig. 5. Worn runway simulation.

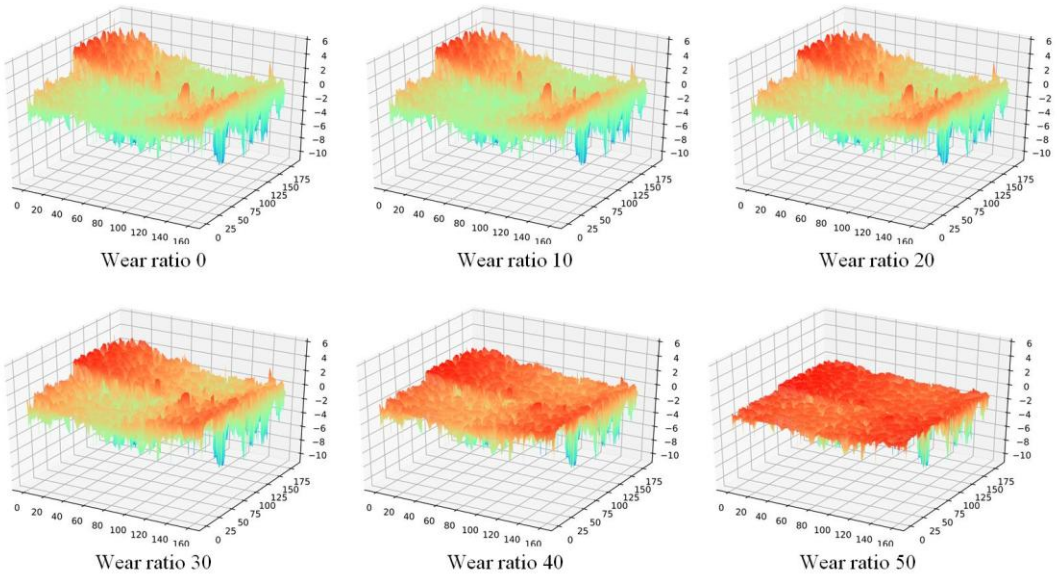

Fig. 6. SMA pavement texture profile with different wear ratios.

The height profiles obtained from the KEYENCE scanning instrument were converted into a runway surface texture model using a python program. The profiles were reorganized using a three-node triangular element (R3D3) and assigned as a rigid surface. Fig. 7 illustrates the asphalt mixture FE models obtained from the scanning results.

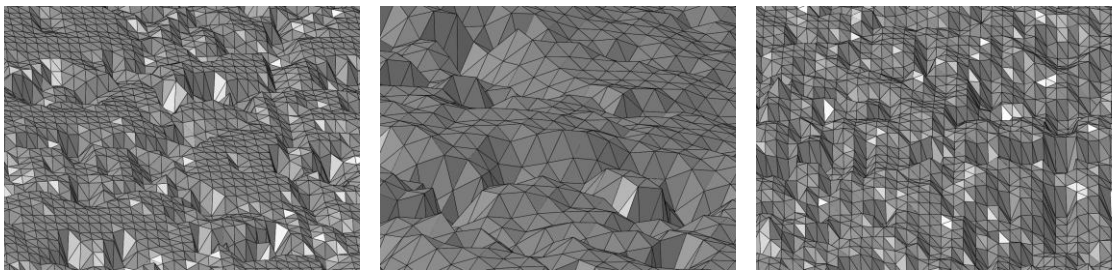

Fig. 7. Asphalt mixture FE models of different gradation.

2.3 Mechanics of rubber–rough runway contact

The contact between a tire and a rough runway surface is predominantly related to the rheological property of the rubber [31]. Eq. (3) presents the kinematic friction coefficient of rubber-like material on wet and dry runways; the coefficient comprises two parts: hysteresis and adhesion parts [32]. Fig. 8 presents the hysteresis friction related to energy dissipation caused by oscillating excitation during sliding on the asperities of asphalt runways. The adhesion force is related to van der Waals interactions between the rubber surface and runway surface. A recent theoretical frictional model provides a relatively clear explanation of hysteresis and adhesion contributions to the interactions between tires and runway tracks，

$$\mu_k = \mu_{Hys} + \mu_{Adh} \tag{3}$$

where μ_k is the kinematic friction coefficient between the rubber and rough runway and μ_{Hys} and μ_{Adh} are friction coefficients caused by hysteresis and adhesion effects, respectively.

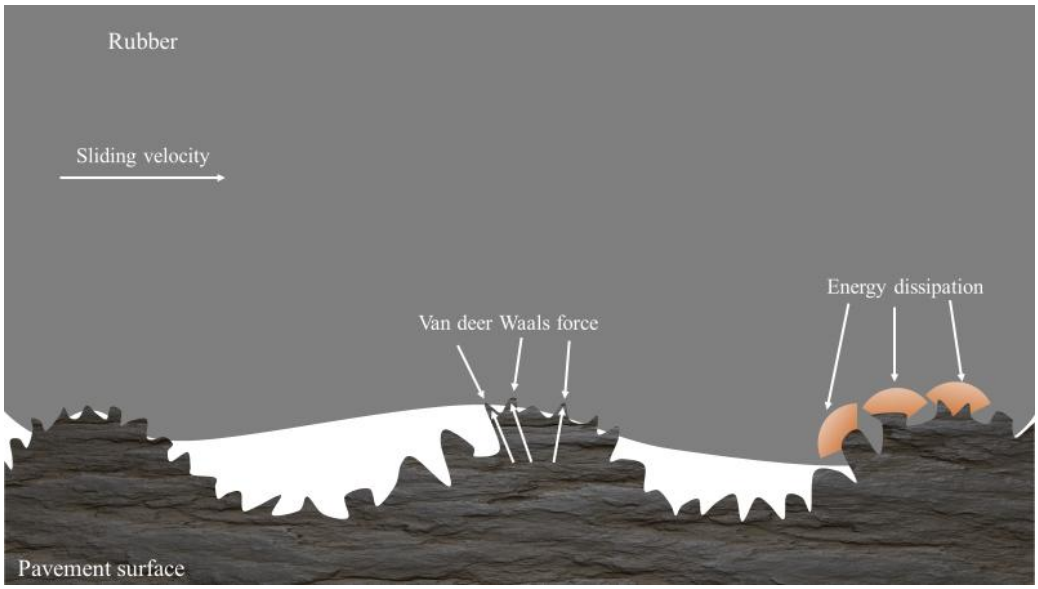

Fig. 8. Generation of friction force.

According to Williamson-Greenwood contact theory, a road surface can be considered to be covered by asperities with identical radii of curvature, R, and with a Gaussian height distribution. However, researchers have proved that asphalt road surfaces exhibit self-affine fractal characteristics and that the texture follows a Gaussian distribution [10, 33]. Because asperities cause the dissipation energy, the hysteresis friction could be calculated by converting surface height profiles into PSD profiles using Fourier transform. Thus, the hysteresis friction coefficient can be expressed as follows:

$$S(f) = \frac{1}{2\pi}\int d^2x\langle h(\bar{x})h(0)\rangle e^{\overline{ifx}} \tag{4}$$

$$\mu_{Hys} = \frac{F_{Hys}}{F_N} = \frac{1}{2(2\pi)^2}\frac{\langle\delta\rangle}{\sigma_0 v_s}\int_{\omega_{min}}^{\omega_{max}} d\omega\omega E^{"}(\omega)S(\omega) \tag{5}$$

where $E^{"}(\omega)$ represents the loss modulus of the tread rubber. $S(\omega)$ denotes the PSD, which can be obtained using morphological results acquired from scanning. Finally, $\langle\delta\rangle$ represents the mean depth of rubber excited by asperities, σ_0 represents the normal stress, ω_{max} represents the maximum excitation frequency related to the minimum asperity, and ω_{min} represents the minimum excitation frequency related to the maximum asperity.

Hysteresis friction is crucial for braking. However, ignoring adhesion friction would cause an underestimation of the actual skid resistance performance of a runway. The adhesion friction coefficient can be obtained using the ratio of the true contact area to the nominal contact area (Eq. (6)):

$$\mu_{Adh} = \frac{F_{Adh}}{F_N} = \frac{\sigma_s}{\sigma_0}\frac{A_c}{A_0} \tag{6}$$

where A_0 is the nominal contact area (i.e., the projection of contact patches). A_c is the real contact area, for which only the top sides of asperities can establish contact with the tire because of the surface texture. Finally, σ_s is the shear stress in the real contact area that results from the molecular energy dissipation of the rubber in the contact patches.

2.4 Rubber–runway friction coefficient

The mean heights of the SMA, AC, and OGFC specimens used in this study were set to zero plane. Fig. 9 presents the height distribution of the specimens, indicating shaper height distributions for the SMA and OGFC specimens compared with the AC specimen. This signifies that the variance of the AC height distribution was larger than that of the SMA and OGFC height distribution, indicating the blunt texture of the AC surface. Fig. 10 illustrates the height distribution of the SMA runway profile with different wear ratios. The height distribution became increasingly asymmetric as the wear ratios increased. The asymmetry indicates that the top sides were abraded by landing traffic.

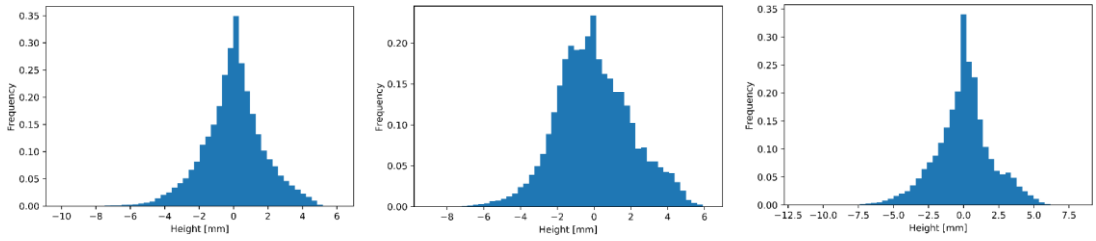

(a) SMA (b) AC (c) OGFC

Fig. 9. Height distribution of different runway textures.

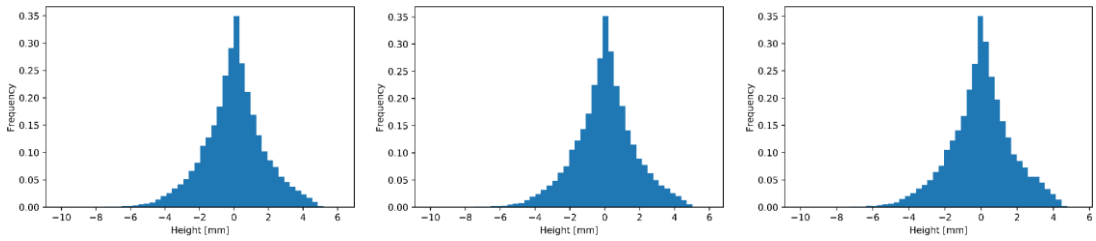

(a) Wear ratio 0 (b) Wear ratio 10 (c) Wear ratio 20

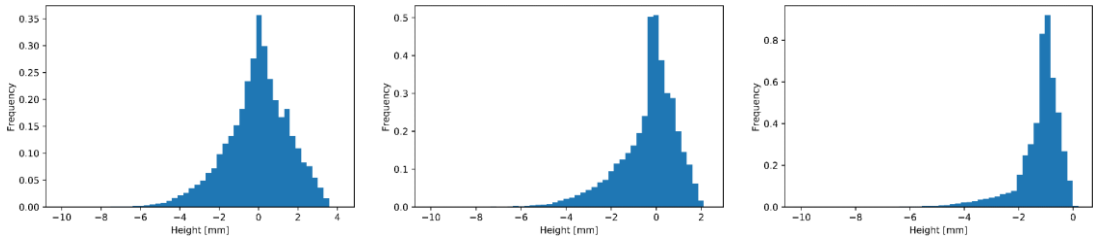

(d) Wear ratio 30 (e) Wear ratio 40 (f) Wear ratio 50

Fig. 10. Height distribution of SMA with different wear ratios.

PSD is a frequency-domain measure of the roughness of a road surface. PSD is derived through the Fourier transform of the correlation function of height profiles; such a function describes roughness distribution with asperity wavelength. This study applied Welch's method to obtain the PSD of runway surface textures. $S(f)$ in Eq. (4) could be obtained by fitting the curves presented in Fig. 9, which illustrates the PSD profiles of the SMA, AC, and OGFC specimens with different wear ratios.

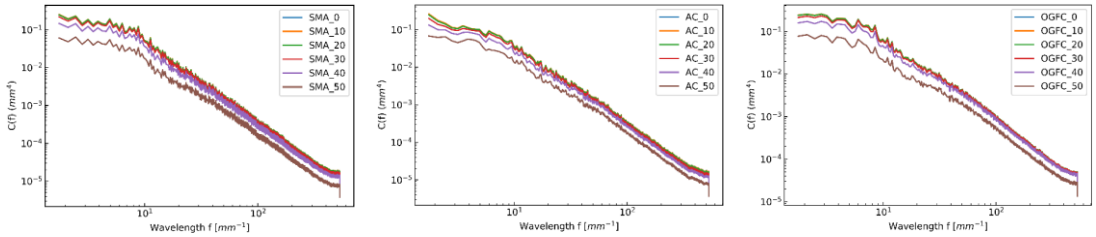

(a) PSD of SMA pavement (b) PSD of AC pavement (c) PSD of OGFC pavement

Fig. 11. PSD of runway textures with different wear ratio.

The coefficient of friction between tire rubber and the runway is affected by surface texture and is related to the viscoelastic property of rubber. The typical viscoelastic property of tread rubber can be obtained from the approaches described in previous studies [29, 30]. Fig. 12 illustrates the real and imaginary parts of the complex modulus of tread rubber.

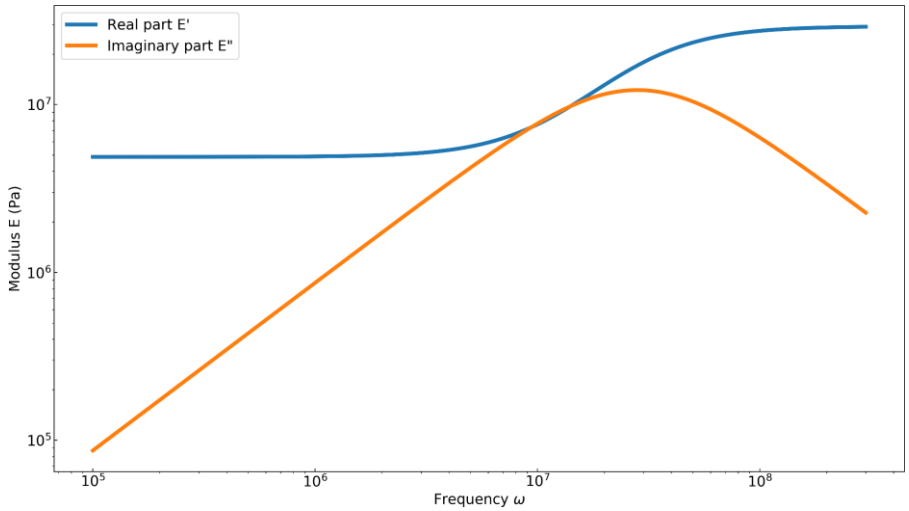

Fig. 12. Viscoelastic modulus of tire rubber.

All parameters required for friction coefficient calculation can be obtained from the PSD and viscoelastic property of rubber materials. The kinematic friction coefficients of specimens can be calculated according to Eqs. (3)–(6). Fig. 13 shows that the material friction coefficients of all specimens in this study decreased as the sliding speed increased. The specimens can be ordered as follows according to their kinematic friction coefficients: OGFC > SMA > AC. The RMS values of the nonworn AC, SMA, and OGFC specimens obtained from scanning were 1.94, 2.11, and 3.21, respectively, and the MPD values of these specimens were 0.61, 0.80, and 1.08, respectively. The derived RMS and MPD values indicate rough surface textures, which caused the differences in the friction coefficients of the specimens. Both indicators are generally influenced by the asphalt mixture gradation. The SMA and AC specimens were continuously graded mixtures containing aggregates of different sizes (ranging from 9.5 to 19 mm). Additionally, the SMA mixture contained a relatively high proportion of coarse aggregates to improve tire grip and rutting resistance. By contrast, the OGFC specimen was an open-graded mixture predominantly containing coarse aggregates to maintain water permeability. Microtexture is typically affected by the texture of aggregates, but macrotexture is affected by the dimension of aggregates. Hence, the RMS and MPD of the mixtures can be attributed to the macrotexture of the mixtures. This explanation is satisfactory because the kinematic friction coefficients of all specimens decreased as the wear ratios increased. However, when the speed was relatively low (<20 m/s), all specimens maintained satisfactory friction coefficients with the increase in wear ratios. The friction

coefficients associated with wear ratios of 0 and 10 were similar; therefore, to simplify the calculation, the condition associated with the wear ratio of 10 was ignored in the FEM model.

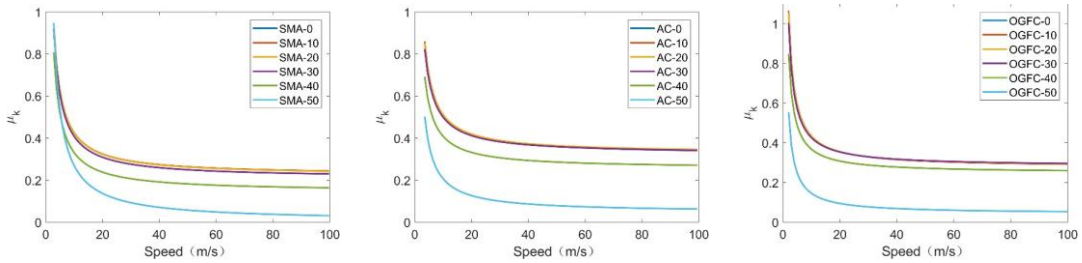

(a) Friction coefficients of SMA pavement with different wear ratios.

(b) Friction coefficients of AC pavement with different wear ratios.

(c) Friction coefficients of OGFC pavement with different wear ratios.

Fig. 13. Kinematic friction coefficients (rubber-runway friction coefficients) of the three types of runways.

3 Results and discussion

3.1 Effect of wear ratios on skid resistance

Before the effects of different parameters on skid resistance were determined, the concept of slip ratio (SR) was defined. During landing, the braking force results from the difference between tire circumferential velocity (v_{tire}) and aircraft velocity ($v_{aircraft}$). SR during aircraft braking is defined as shown in Eq. (7). SR values of 100 and 0 represent fully locked and free roll tires, respectively.

$$\mathrm{SR} = \frac{v_{aircraft} - v_{tire}}{v_{aircraft}} \times 100 \tag{7}$$

This study considered different SRs, four aircraft velocities (55, 105, 155, and 205 km/h), and different wear ratio conditions (0, 20, 30, 40, and 50). Fig. 14 illustrates the effect of SR on dry friction coefficients. It should be noted that the friction coefficient mentioned here is the effective tire to runway friction coefficient, which is calculated by the FEM simulation and the rubber-runway friction coefficients shown in Fig.13 are used as the FEM input parameters. To make it clearer, the dry friction coefficient mentioned here is marked as μ_{eff_dry}.The μ_{eff_dry} increased initially with an increase in SR under different wear ratios. When the optimal SR reached 20%, the friction coefficient decreased with the SR. This finding signifies that the

maximum friction coefficient can be achieved at the optimal SR. Therefore, the antilock braking system (ABS) of an aircraft should maintain the optimal SR during landing to retain sufficient braking force. However, the optimal SR is not a constant value; it changes with wear ratios and speeds. The μ_{eff_dry} curves in this study generally decreased with an increase in the wear ratio. Moreover, the changing trend increased with the wear ratio. When the optimal SR was approximated, the changing trend of the μ_{eff_dry} increased with the landing speed. The ridges of the friction curves became steeper as the landing speed increased. Accordingly, the ABS of an aircraft must be precisely controlled because friction force is substantially lost when the SR exceeds its optimum range. Similar results were observed for the AC-13 and OGFC-13 runway surfaces.

Under various SRs, surface texture degradation was determined to have different effects on friction coefficients. For example, as displayed in Fig. 14 (a), the differences in friction coefficients between the excessive slip state (approximately 10% SR) and insufficient slip state (approximately 90% SR) of the new runway (SMA-0) and worn-out runway (SMA-50) were 0.03 and -0.07, respectively. This indicates that the effect of the wear ratio on the excessive slip state was greater than that on the insufficient slip state.

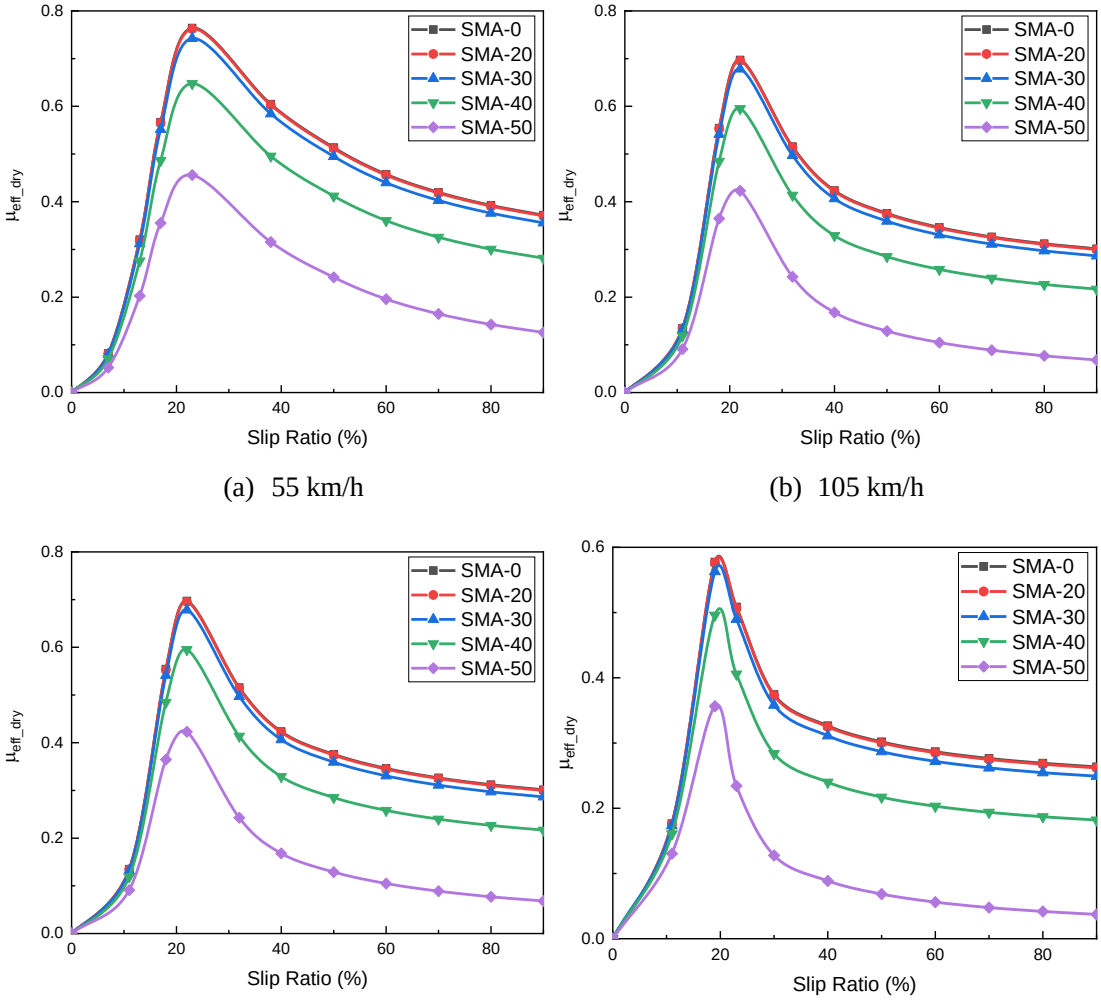

Fig. 14. Friction coefficient versus SR at the SMA pavement with different wear ratios.

The optimal friction coefficient is defined as the largest friction coefficient at an SR of 20. Because an ABS controls aircraft braking, analyzing the optimal friction coefficient would be more practical. As presented in Fig. 15, the optimal friction coefficient decreased with an increase in the wear ratio. The decreasing rate also increased with the wear ratio. Additionally, at a high landing speed (205 km/h), the reduction in friction coefficients between long-serving (wear ratio 50) and new SMA runways (wear ratio 0) was 0.22; furthermore, the reductions in friction coefficients between long-serving and new AC runways and between long-serving and new OGFC runways were 0.23 and 0.26, respectively. At a low landing speed (55 km/h), the differences between the friction coefficients of long-serving (wear ratio 50) and new (wear ratio 0) SMA, AC, and OGFC runways were 0.31, 0.32, and 0.38, respectively. On the basis of these results, one can conclude that the effect of wear on low-speed landing is greater than that on high-speed landing.

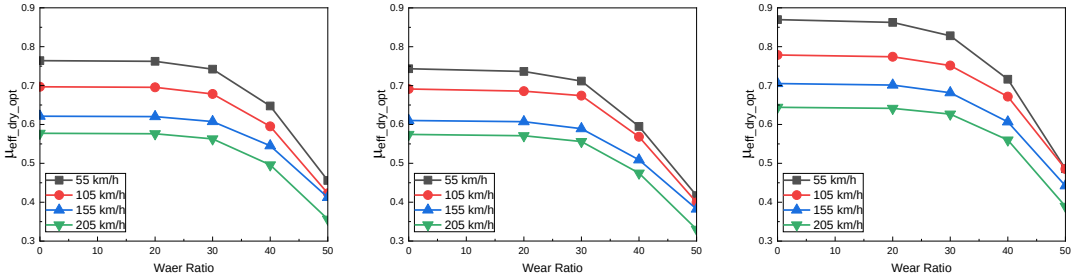

(a) SMA (b) AC (c) OGFC

Fig. 15. Optimal friction coefficients versus wear ratios of the three types of runways.

3.2 Effect of runway type on optimal friction coefficients

The three asphalt samples can be ordered as follows according to their friction coefficients: OGFC > SMA > AC. Under different wear ratios, the optimal friction coefficient of the OGFC asphalt runway was considerably higher than those of the AC and SMA asphalt runways. This signifies that the surface roughness of the OGFC was greater than that of the AC and SMA. As displayed in Fig. 16, under dry runway conditions, the differences in optimal friction coefficients between the three asphalt runways decreased as the wear ratio increased. At a speed of 55 km/h, the friction coefficients of the SMA and AC decreased by 0.11 and 0.13 compared with the OGFC, respectively. After surface textures had been abraded through a wear simulation, the skid resistance properties of the different runways coincided with each other. At a speed of a 205 km/h, the friction coefficients of the SMA and AC samples decreased by 0.03 and 0.07 compared with the OGFC samples, respectively. The three specimens exhibited similar micro-textures because the same aggregates were used for these three specimens. However, the OGFC specimen exhibited larger macrotextures because of the presence of more coarse aggregates; pavement macrotextures highly depend on the larger macrotexture depth, which is influenced by aggregate dimensions. Among the three specimen types, the OGFC specimen exhibited the highest skid resistance, which can be attributed to the coarse aggregates. However, because macrotextures were deteriorated through the wear simulation, the difference in skid resistance properties between the three runway types decreased.

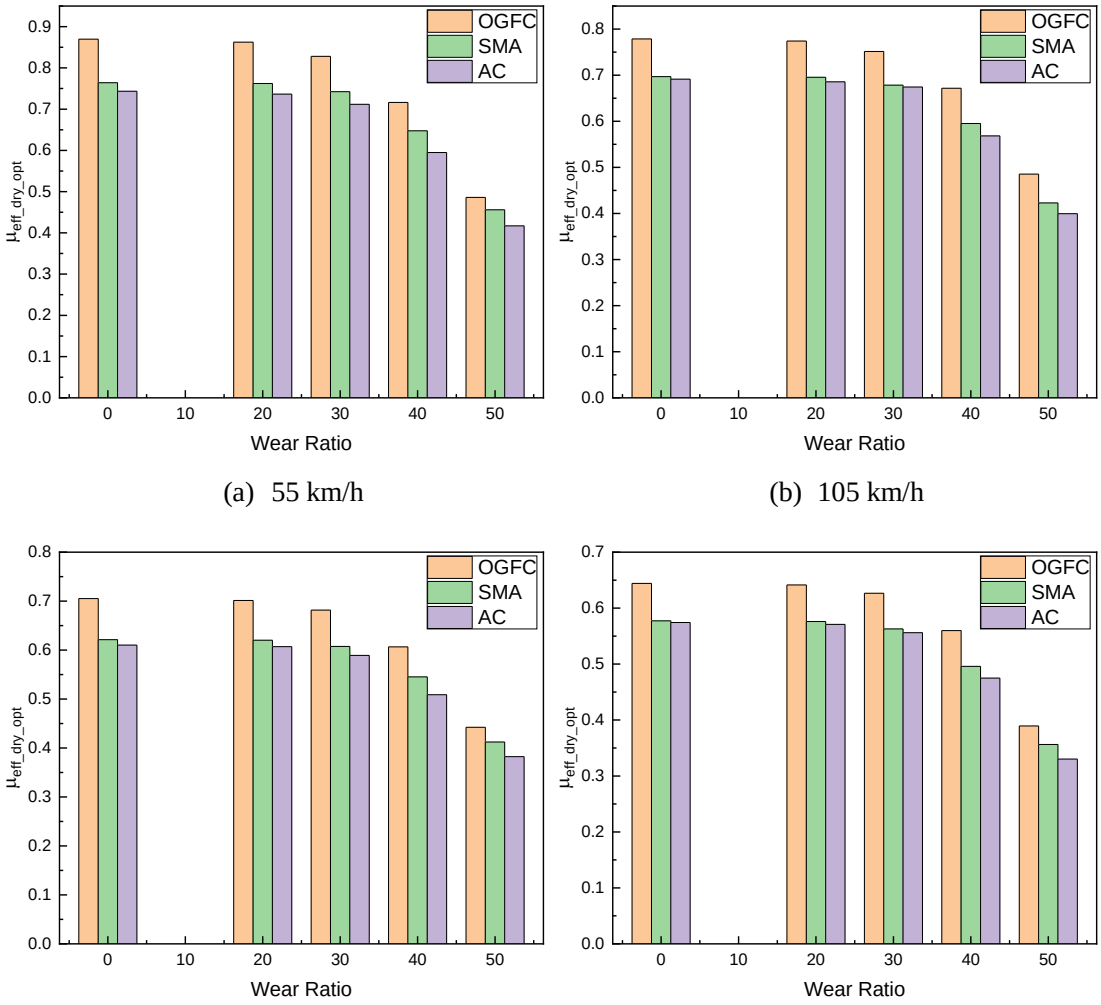

Fig. 16. Optimum friction coefficients of the three specimens with different velocities.

3.3 Effect of water film depth on hydroplaning speed

At a relatively high landing speed, hydrodynamic force could increasingly lead to the detachment of tires from wet runways. Therefore, tire–runway contact is critical for safe aircraft landing. In the FE simulation in this study, the speed was set to the range of 30–300 km/h. The simulation involved dry and wet runways with water depths of 2–8 mm. Hydroplaning speed is defined as the speed causing a contact force loss of 95% on wet runways.

The tire–runway contact force was obtained from the simulation (Fig. 17); the contact force on the dry runway remained constant, whereas that on the wet runway decreased at higher landing speeds. At a speed of 50 km/h, the contact force decreased by 9%–17% for water depths of 2–8 mm. At a speed of 150 km/h, the contact force decreased by 32%–94% for water depths of 2–8

mm. This finding indicates that the contact force at high landing speeds was strongly influenced by the water depth. At speeds of 30–300 km/h, the contact force for a water depth of 2 mm decreased by 0.3%–74%. Moreover, when the landing speed was below 300 km/h, the aircraft tires did not cause hydroplaning on the wet runway at the 2-mm water depth. Accordingly, the hydroplaning speed of aircraft tires could decrease with an increase in water film thickness. In particular, when the water depth exceeded 5 mm, the hydroplaning speed decreased rapidly from 237 to 182 km/h.

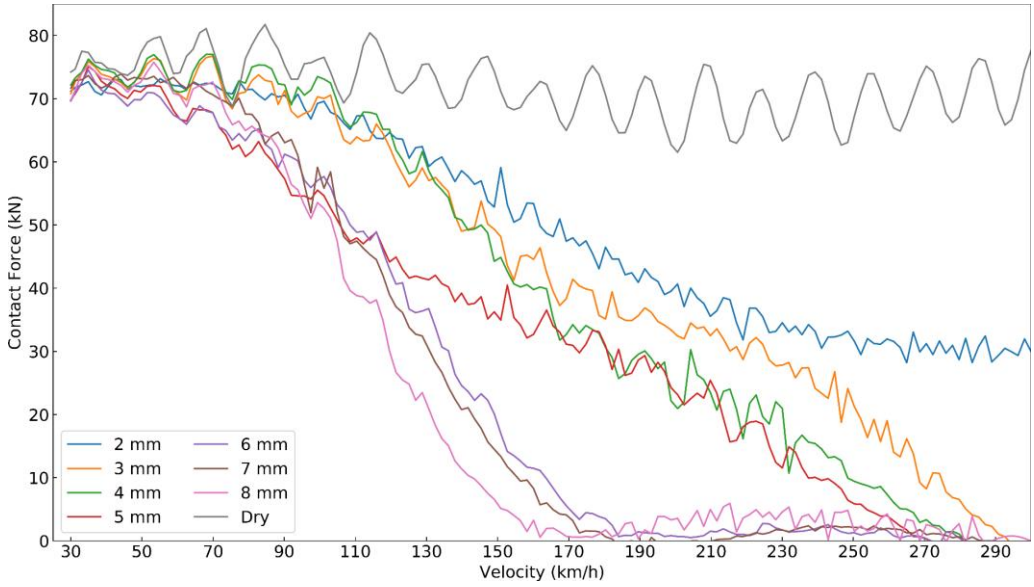

Fig. 17. Contact force between tires and runways at different water depths.

Fig. 18 illustrates the footprints of aircraft tires during hydroplaning, as obtained from the FE simulation. The simulation results were compared with experimental results reported by Horne [34]. Horne conducted experiments on a glass plate with a 10-mm water depth and using a vehicle tire with a 378-kg vertical load; by contrast, the simulation in the present study was conducted on runways with a 5-mm water depth and using an aircraft tire with a 6600-kg vertical load. Nevertheless, the results regarding the hydroplaning phenomenon were quite similar between the two studies; for example, footprints obtained from the numerical simulation were nearly identical to those from the experiments. Water was evacuated from the grooves and sides of the tire at a low speed (Fig. 18). Subsequently, water started wedging into the tire–runway interface at a higher speed. Finally, the tire was detached from the runway because its speed exceeded hydroplaning speed.

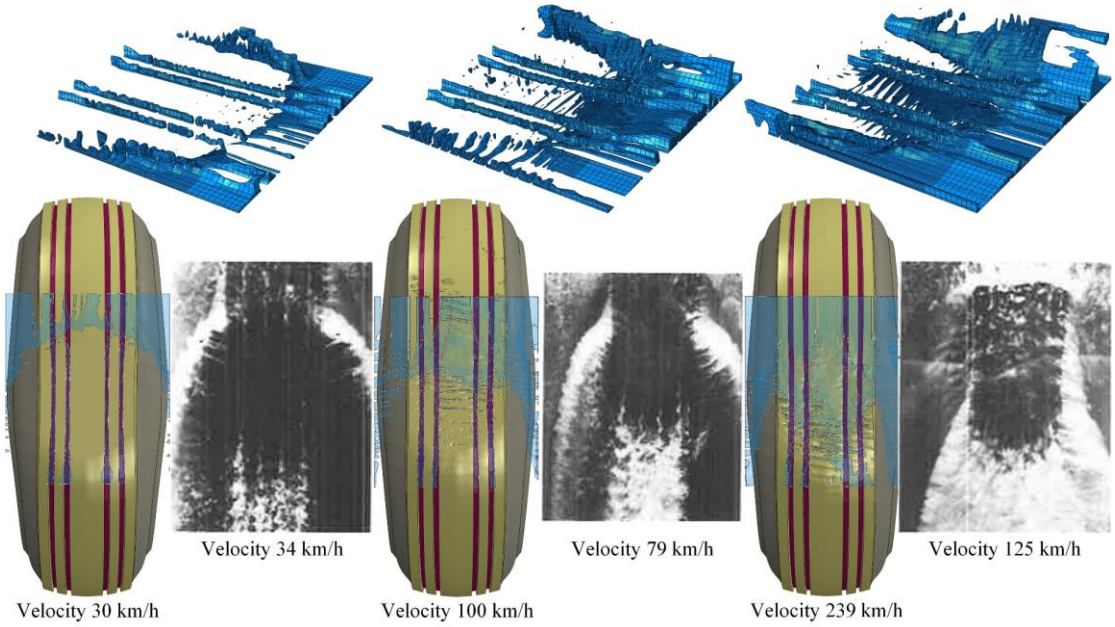

Fig. 18. Progressive development of hydroplaning obtained from simulations and experiments.

3.4 Effect of water film depth on optimal friction coefficients

Complete hydroplaning is a rare phenomenon that involves loss of controllability and braking efficiency caused by an uplift force when the landing speed of an aircraft exceeds the hydroplaning speed on wet runways. Partial hydroplaning is a phenomenon in which tires are partially detached from a wet runway when the landing speed of an aircraft remains within the hydroplaning speed on the wet runway. Partial hydroplaning is highly common and is usually caused by a considerable friction loss. Therefore, partial hydroplaning cannot be ignored because it can substantially increase the landing distance due to thick water film depths and high landing speeds. To investigate the phenomenon of partial hydroplaning, the friction between the tires and wet runway surface should be determined, as defined in Eq. (8), which has commonly been used in previous studies [26, 28, 35]. In this equation, μ_{eff_wet} is the friction coefficient on a wet runway and μ_{eff_dry} is the friction coefficient on a dry runway, which can be obtained using the proposed FE model. L is the aircraft load and F is the hydrodynamic force, which can be obtained using the FE model.

$$\mu_{eff\_wet} = \frac{\mu_{eff\_dry} \times (L-F)}{L} \tag{8}$$

In this study, the friction coefficients of new (wear ratio = 0) and long-serving (wear ratio = 50) SMA runways were calculated according to the FE model; as illustrated in Fig. 19(a)–(c), the

friction curves decreased with an increase in landing speed during partial hydroplaning. The decreasing rate of friction increased depending on the water film depth. Compared with dry runway, the decreasing rates of runway with 3mm and 5 mm water film were 5.8% and 10.6% with landing velocity 55 km/h. However, the decreasing rates of runway with 3mm and 5 mm water film were 63.6% and 65.4% with landing velocity 205 km/h. In particular, when the aircraft landing speed was 205 km/h and water film depth was 5 mm, the friction coefficient was generally <0.1. The friction of the worn-out wet runway also decreased compared with that of the new runway. The friction coefficient at the 205-km/h landing speed and 5-mm water-film depth was <0.05 (Fig. 19(f)). Both cases indicate extremely dangerous landing scenarios with a small traction force.

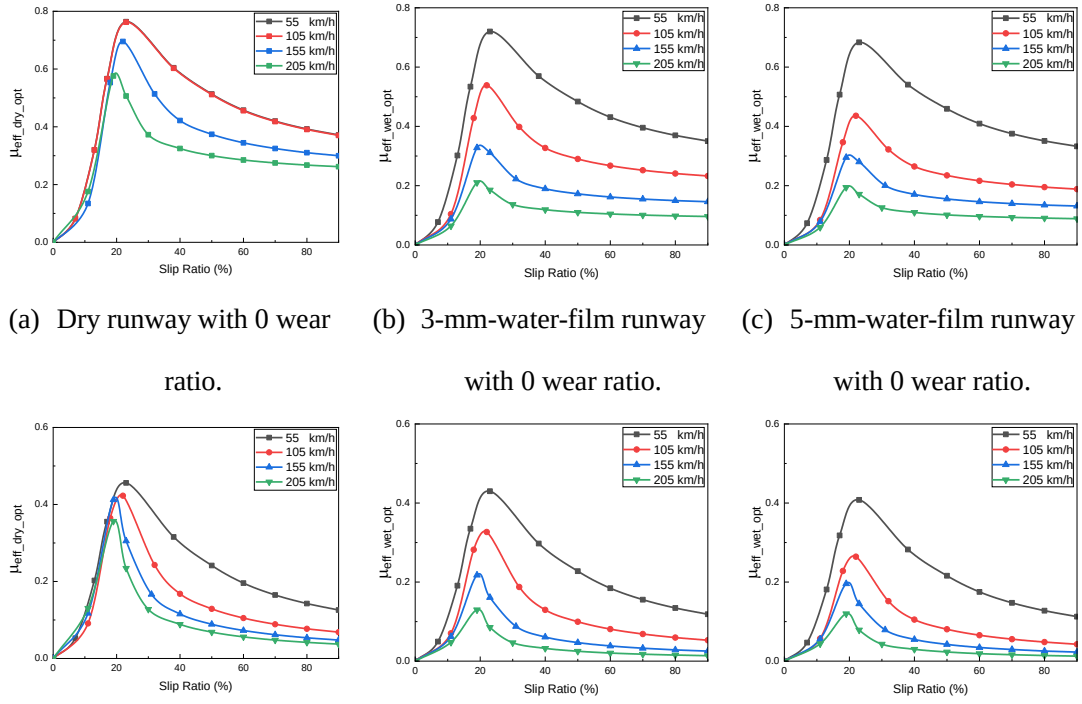

(a) Dry runway with 0 wear ratio. (b) 3-mm-water-film runway with 0 wear ratio. (c) 5-mm-water-film runway with 0 wear ratio.

(d) Dry runway with 50 wear ratio. (e) 3-mm-water-film runway with 50 wear ratio. (f) 5-mm-water-film runway with 50 wear ratio.

Fig. 19. Optimal friction coefficients versus slip ratios on wet SMA runways.

To study landing processes controlled by an ABS, the optimal friction of dry and wet runways were obtained from the FE model. As displayed in Fig. 20, the optimal friction coefficients decreased linearly as the landing speed increased. The slopes of the friction curves also increased as the water film depth increased. Compared with that on the dry runway, the friction coefficients on the wet runway at water depths of 3 and 5 mm and a wear ratio of 0

decreased by 0.36 and 0.38, respectively. Additionally, the loss of coefficient was 0.31 for the worn runway (wear ratio 50). This finding indicates that partial hydroplaning and lack of surface textures could endanger landing safety because of a lack of skid resistance.

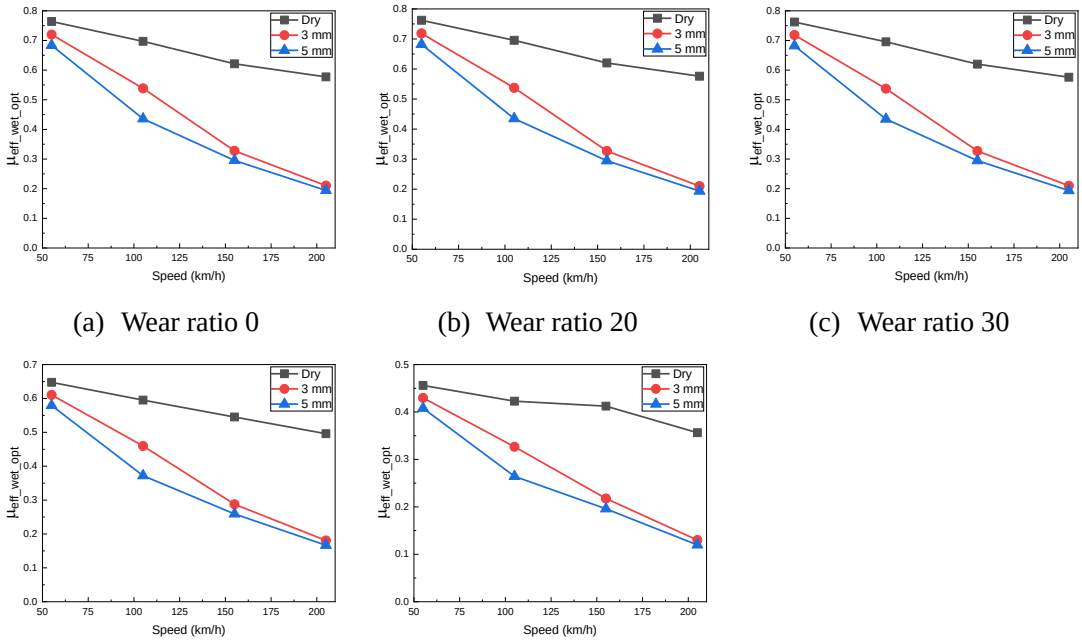

(a) Wear ratio 0 (b) Wear ratio 20 (c) Wear ratio 30

(d) Wear ratio 40 (e) Wear ratio 50

Fig. 20. Optimal friction coefficients of SMA runway.

4 Conclusions

This study developed an integrated modelling approach to quantify the skid resistance of wet and dry runways based on tribology theory, a texture wear algorithm, and a hydroplaning model. The kinematic friction coefficients between tread rubber materials and rough runways were obtained using the PSD of pavements and viscoelastic property of rubber. An FE model was developed according to real texture surface and real interaction models. Factors influencing the coefficient of effective friction between aircraft tires and runways were analyzed. The following conclusions were drawn:

(1) The effective runway friction coefficient decreases with an increase in the aircraft landing speed, and the optimal friction coefficient decreases with an increase in the landing speed.

(2) The three types of runways in this study can be ordered as follows according to their

effective friction coefficients: OGFC > SMA > AC. Compared with the new OGFC specimen, the effective friction coefficients of the new SMA and AC specimens decreased by 0.11 and 0.13 at a landing speed of 55 km/h, respectively. However, compared with the same worn-out OGFC specimen, the effective friction coefficients of the worn-out (wear ratio 50) SMA and AC specimens decreased by 0.03 and 0.06 at a landing speed of 55 km/h, respectively. Accordingly, the difference in skid resistance properties between the OGFC, SMA, and AC specimens decreased as the wear ratio increased.

(3) The optimal friction coefficient decreased as the wear ratio increased. The reductions in the optimal friction coefficients of the SMA, OGFC, and AC specimens between long-serving and new runways were 0.22, 0.24, and 0.26, respectively, at a high landing speed of 205 km/h. The reductions in the optimal friction coefficients of the SMA, AC, and OGFC pavements were 0.31, 0.33 and 0.38 at the high landing speed of 205 km/h. Therefore, the effect of wear at a low landing speed is greater than that at a high landing speed.

(4) Compared with the dry runway, the effective friction coefficients of the wet runway decreased by 0.36 and 0.38 when partial hydroplaning occurred on the wet runway at water film depths of 3 and 5 mm, respectively, and landing speed of 205 km/h; however, the effective friction coefficients decreased by 0.04 and 0.08, respectively, at a landing speed of 55 km/h. Therefore, partly hydroplaning is more obvious at a high landing speed than at a low landing speed.

The FE model demonstrated in this paper provides a convenient tool for analyzing runway skid resistance. However, in the model, only water drainage provided by tires is considered; water drainage provided by runway textures and thermal effect of rubber are not considered. This could be the focus of future simulation work.

Acknowledgments

The work described in this paper is supported by the National Natural Science Foundation of China (Nos. U1633116, 51922079, 61911530160), Shanghai Pujiang Program, and the Fundamental Research Funds for the Central Universities.

References

[1] Gunaratne M, Bandara N, Medzorian J, Chawla M, Ulrich P. Correlation of Tire Wear and Friction to Texture of Concrete Pavements. Journal of Materials in Civil Engineering. 2000;12:46-54.

[2] Henry JJ. Evaluation of pavement friction characteristics: Transportation Research Board; 2000.

[3] Mahboob Kanafi M, Kuosmanen A, Pellinen TK, Tuononen AJ. Macro-and micro-texture evolution of road pavements and correlation with friction. International Journal of Pavement Engineering. 2015;16:168-79.

[4] Es GWHV. Running out of runway: analysis of 35 years of landing overrun accidents. National Aerospace Laboratory NLR2005.

[5] Joyner UT, Horne WB, Leland TJ. Investigations on the Ground Performance of Aircraft Relating to Wet Runway Braking and Slush Drag. ADVISORY GROUP FOR AERONAUTICAL RESEARCH AND DEVELOPMENT PARIS (FRANCE); 1963.

[6] Pasindu HR, Fwa TF. Improving Wet-Weather Runway Performance Using Trapezoidal Grooving Design. Transportation in Developing Economies. 2015;1:1-10.

[7] Zelelew H, Khasawneh M, Abbas A. Wavelet-based characterisation of asphalt pavement surface macro-texture. Road Materials and Pavement Design. 2014;15:622-41.

[8] Kane M, Zhao D, Do M-T, Chailleux E, De-Lalarrard F. Exploring the ageing effect of binder on skid resistance evolution of asphalt pavement. Road materials and pavement design. 2010;11:543-57.

[9] Do MT, Tang Z, Kane M, de Larrard F. Evolution of road-surface skid-resistance and texture due to polishing. Wear. 2009;266:574-7.

[10] Villani MM, Scarpas A, de Bondt A, Khedoe R, Artamendi I. Application of fractal analysis for measuring the effects of rubber polishing on the friction of asphalt concrete mixtures. Wear. 2014;320:179-88.

[11] Kogbara RB, Masad EA, Kassem E, Scarpas A, Anupam K. A state-of-the-art review of parameters influencing measurement and modeling of skid resistance of asphalt pavements. Construction and Building Materials. 2016;114:602-17.

[12] Flintsch GW, de León E, McGhee KK, AI-Qadi IL. Pavement Surface Macrotexture

Measurement and Applications. Transportation Research Record. 2003;1860:168-77.

[13] Vaiana R, Capiluppi GF, Gallelli V, Iuele T, Minani V. Pavement Surface Performances Evolution: an Experimental Application. Procedia - Social and Behavioral Sciences. 2012;53:1149-60.

[14] Kane M, Artamendi I, Scarpas T. Long-term skid resistance of asphalt surfacings: Correlation between Wehner–Schulze friction values and the mineralogical composition of the aggregates. Wear. 2013;303:235-43.

[15] Ivan JN, Ravishanker N, Jackson E, Aronov B, Guo S. A Statistical Analysis of the Effect of Wet-Pavement Friction on Highway Traffic Safety. Journal of Transportation Safety & Security. 2012;4:116-36.

[16] Srirangam S, Anupam K, Scarpas A, Kasbergen C, Kane M. Safety aspects of wet asphalt pavement surfaces through field and numerical modeling investigations. Transportation Research Record: Journal of the Transportation Research Board. 2014:37-51.

[17] Dreher RC, Horne W. Phenomena of pneumatic tire hydroplaning. Skidding. 1963.

[18] Forster SW. Pavement microtexture and its relation to skid resistance. Transportation research record. 1989;1215:151-64.

[19] Gallaway BM, Schiller RE, Rose JG. The effects of rainfall intensity, pavement cross slope, surface texture, and drainage length on pavement water depths. 1971.

[20] Anderson DA, Huebner R, Reed JR, Warner J, Henry JJ. Improved surface drainage of pavements. 1998.

[21] Žmindák M, Grajciar I. Simulation of the aquaplane problem. Computers & Structures. 1997;64:1155-64.

[22] Ong GP, Fwa TF. Wet-Pavement Hydroplaning Risk and Skid Resistance: Modeling. Journal of Transportation Engineering. 2007;133:590-8.

[23] Fwa TF, Ong GP. Wet-Pavement Hydroplaning Risk and Skid Resistance: Analysis. Journal of Transportation Engineering. 2008;134:182-90.

[24] Zhang L, Fwa TF, Ong GP, Chu L. Analysing effect of roadway width on skid resistance of porous pavement. Road Materials and Pavement Design. 2016;17:1-14.

[25] Pasindu H, Fwa T, Ong G. Analysis of skid resistance variation on a runway during an aircraft landing operation. Seventh International Conference on Maintenance and Rehabilitation of Pavements and Technological Control2012.

[26] Anupam K, Kumar SS, Kasbergen C, Scarpas A, Kane M. Finite Element Framework for the Computation of Runway Friction of Aircraft Tires. Transportation Research Record. 2017:126-38.

[27] Srirangam SK, Anupam K, Kasbergen C, Scarpas AT. Analysis of asphalt mix surface-tread rubber interaction by using finite element method. Journal of Traffic and Transportation Engineering (English Edition). 2017;4:395-402.

[28] Srirangam SK, Anupam K, Kasbergen C, Scarpas A, Cerezo V. Study of Influence of Operating Parameters on Braking Friction and Rolling Resistance. Transportation Research Record: Journal of the Transportation Research Board. 2015:79-90.

[29] Liu X, Cao Q, Wang H, Chen J, Huang X. Evaluation of Vehicle Braking Performance on Wet Pavement Surface using an Integrated Tire-Vehicle Modeling Approach. Transportation Research Record. 2019;2673:295-307.

[30] Zhu SZ, Liu XY, Cao QQ, Huang XM. Numerical Study of Tire Hydroplaning Based on Power Spectrum of Asphalt Pavement and Kinetic Friction Coefficient. Advances in Materials Science and Engineering. 2017:1-11.

[31] Popov VL. Contact mechanics and friction: Springer; 2010.

[32] Heinrich G, Klüppel M. Rubber friction, tread deformation and tire traction. Wear. 2008;265:1052-60.

[33] Chen XH, Wang DW. Fractal and spectral analysis of aggregate surface profile in polishing process. Wear. 2011;271:2746-50.

[34] Horne WB. Tire hydroplaning and its effects on tire traction. Highway Research Record. 1968.

[35] Srirangam S. Numerical Simulation of Tire-Pavement Interaction: TU Delft; 2015.

***Declaration of Interest Statement**

Declaration of interests

☒ The authors declare that they have no known competing financial interests or personal relationships that could have appeared to influence the work reported in this paper.

☐The authors declare the following financial interests/personal relationships which may be considered as potential competing interests: